LAWRENCE
LIVERMORE
NATIONAL
LABORATORY

LLNL-JRNL-413738

Network Sensitivity Solutions for Regional Moment Tensor Inversions

S. R. Ford, D. S. Dreger, W. R. Walter

June 9, 2009

Bulletin of the Seismological Society of America

Disclaimer

This document was prepared as an account of work sponsored by an agency of the United States government. Neither the United States government nor Lawrence Livermore National Security, LLC, nor any of their employees makes any warranty, expressed or implied, or assumes any legal liability or responsibility for the accuracy, completeness, or usefulness of any information, apparatus, product, or process disclosed, or represents that its use would not infringe privately owned rights. Reference herein to any specific commercial product, process, or service by trade name, trademark, manufacturer, or otherwise does not necessarily constitute or imply its endorsement, recommendation, or favoring by the United States government or Lawrence Livermore National Security, LLC. The views and opinions of authors expressed herein do not necessarily state or reflect those of the United States government or Lawrence Livermore National Security, LLC, and shall not be used for advertising or product endorsement purposes.

Network sensitivity solutions for regional moment tensor inversions

Sean R. Ford [a], Douglas S. Dreger [b], William R. Walter [a]

[a] Lawrence Livermore National Laboratory, Livermore, California 94550, USA
[b] Berkeley Seismological Laboratory, Berkeley, California 94720, USA

Abstract

Well-resolved moment tensor solutions reveal information about the sources of seismic waves. Here we introduce a new way of assessing confidence in the regional full moment tensor inversion via the introduction of the network sensitivity solution (NSS). The NSS takes into account the unique station distribution, frequency band, and signal-to-noise ratio of a given event scenario. The NSS compares both a hypothetical pure source (for example an explosion or an earthquake) and the actual data with several thousand sets of synthetic data from a uniform distribution of all possible sources. The comparison with a hypothetical pure source provides the theoretically best-constrained source-type region for a given set of stations, and with it one can determine whether further analysis with the data is warranted. The NSS that employs the actual data gives a direct comparison of all other source-types with the best-fit source. In this way, one can choose a threshold level of fit where the solution is comfortably constrained. The method is tested for the well-recorded nuclear test, JUNCTION, at the Nevada Test Site. Sources that fit comparably well to a hypothetical pure explosion recorded with no noise at the JUNCTION data stations have a large volumetric component and are not described well by a double-couple (DC) source. The NSS using the real data from JUNCTION is even more tightly constrained to an explosion since the data contains some energy that precludes fitting with any type of deviatoric source. We also calculate the NSS for the October 2006 North Korea test and a nearby earthquake, where the station coverage is poor and the event magnitude is small. The earthquake solution is very well fit by a DC source, and the best-fit solution to the nuclear test (M_W4.1) is dominantly explosion.

1. Introduction

Ford et al. (2009) calculated seismic moment tensors for 17 nuclear test explosions, 12 earthquakes, and 3 collapses in the vicinity of the Nevada Test Site in the Western US. They found that the relative amount of isotropic and deviatoric moment provided a good discriminant between the explosions and earthquakes. The observational work to describe the discriminant was accompanied by a theoretical study into the sensitivities of the method and it was found that the ability to resolve a well-constrained solution is dependent on station configuration, data bandwidth, and signal-to-noise ratio (SNR). It is difficult to state steadfast rules for what source-types can be resolved for all conditions, when different conditions lead to different levels of confidence in the solution. Therefore, in this study we develop a confidence analysis specific to the source type, station configuration and data SNR, which we call the network sensitivity solution (NSS).

There have been many attempts to understand error in seismic moment tensor inversions. Sileny and coathors have done extensive sensitivity testing of the methods they use to calculate the moment tensor. Sileny et al. (1992; 1994), Sileny (1998), Jechumtalova and Sileny (2001, 2005), Sileny and Vavrycuk (2002), and Sileny (2004) have collectively investigated the effects of incorrect event depth, poor knowledge of the structural model including anisotropy, noise, and station configuration on the retrieved solution. They found that for only a few stations with data of SNR>5 the moments of various components were sensitive to improper source depth and velocity model, but that the mechanism remained robust, and that spurious isotropic components may manifest in the solution if an isotropic medium assumption is made incorrectly. Roessler et al. (2007) confirm this last result. The probabilistic inversion method by Weber (2006) using near-field full-waveform data helped to inspire the approach taken in this study. Weber (2006) inverts for hundreds of sources using a distribution of hypocentral location based on *a priori* information. Perturbations to the velocity model and noise are also added in the synthetic portion of the study. Empirical parameter distributions are then produced to assess the resolution. Mechanism distribution is plotted with a Riedesel and Jordan (1989) plot, which is also the preference of many of the previously mentioned studies. In the following study we will employ the source-type plot from Hudson et al. (1989), which is described in Ford et al. (2009). Further details of the inversion method and its practical implementation are also given in Ford et al. (2009).

We first test the NSS methodology on a well-studied earthquake and explosion at the Nevada Test Site (NTS) and then implement it for the 9 Oct 06 North Korea nuclear test. The recent 25 May 09 North Korea explosion has very similar waveforms to the 2006 test at the stations employed in this study, but they are around 4-6 times larger. Therefore, the 2006 explosion is a better test of the NSS method for discriminating small explosions, which is an active area of research in explosion monitoring.

2. Data and Method

The NSS is first performed for an aftershock of the Little Skull Mt. earthquake (M_L4.2, 5 Jul 92) and the JUNCTION nuclear test (M_L4.8, 26 Mar 92), both of which took place at NTS and were analyzed in Ford et al. (2009). Three-component recordings of the earthquake and explosion

were collected from eight and six stations, respectively, from the Berkeley Digital Seismic Network, Trinet, and the Lawrence Livermore National Laboratory (LLNL) network. Locations of the events and stations are given in Figure 1a. All data is freely available from IRIS via the internet except the LLNL historic network data, which is available on compact disk (Walter et al., 2006). We remove the instrument response, rotate to the great-circle frame, integrate to obtain displacement, and filter the data with a 4-pole acausal Butterworth filter with a low-corner of 50 sec and a high-corner of 20 sec, except for the LLNL network (composed of Sprengnether instruments with limited long-period response), which is filtered between 10 and 30 sec. The full-waveform regional data is inverted in the time-domain for the complete moment tensor as described in Minson and Dreger (2009). The Green's functions (GFs) used in the inversion are for a one-dimensional (1-D) velocity model of eastern California and western Nevada (Song et al., 1996) where the source for the earthquake is near the catalog depth of 7 km and the explosion is at 1km depth. We use these GFs to produce two types of NSSs, a theoretical NSS and an actual NSS.

The theoretical NSS tries to answer the question of how well a pure earthquake or explosion can be resolved with very high signal-to-noise ratio (SNR) data for the given event scenario (i.e., data bandwidth and station distribution). To do this we use the GFs to first produce data for a model event (earthquake or explosion) as well as a uniform distribution of synthetic sources representing all possible sources, where the moment of these sources is chosen so as to best fit the model event data. In the case of an earthquake, a uniform distribution of double-couple mechanisms is used as the model event (Figure S1a).

The source-type parameters (Hudson et al., 1989) are calculated for each synthetic source (Figure S1b). Since the source-type plot does not account for total seismic moment (only relative moment) or source orientation, a single set of source-type parameters (one point on the source-type plot) can represent several sources. For example, a DC source with any strike, rake, or dip, will plot in the center of the source-type plot (Figure S1c). However, as one moves away from the center of the source-type plot (location of a DC mechanism), source orientation becomes less important to the seismic radiation so that the top and bottom of the plot are uniquely represented by an explosion or implosion, respectively.

The model event data d is then compared with the synthetic source data s and the fit for each comparison is quantified by the variance reduction VR

$$\mathrm{VR} = \left[1 - \frac{\sum_i (d_i - s_i)^2}{\sum_i d_i^2} \right] \times 100 \,. \qquad (1)$$

where i are the displacements at all times for all components at all stations.

The VR for each synthetic source is calculated and plotted as a function of source-type parameter on the source-type plot. Since a single set of source-type parameters can represent many sources that could have varying levels of fit to the model event data (and therefore, VR), a moving-maximum window is used to smooth the VR distribution. The source-type plot empirical VR

distributions are shown in Figure S2a for the Little Skull Mt. aftershock and Figure 2a for the JUNCTION explosion.

The actual NSS tries to find what source can be reliably resolved for the given event scenario. The actually recorded data is used in place of the model explosion data, which is compared with the same synthetic dataset of all possible sources to produce empirical VR distributions on the source-type plot as in Figure S2b for the Little Skull Mt. aftershock and Figure 2b for the JUNCTION explosion.

The North Korea nuclear test (m_b4.2, 9 Oct 06) and a nearby earthquake that occurred on 16 Dec 04 is also analyzed with records from four stations that recorded the events well in the period band of interest (Figure 1b). The same data processing steps are followed as previously described except that the earthquake and explosion data for three of the stations (INCN, TJN, and BJT) are filtered between 15 to 30 sec, and 10 to 20 sec, respectively, and data from station MDJ is filtered between 15 to 50 sec, and 10 to 50 sec, respectively, in order to increase the SNR. The GFs for these events are derived from the MDJ2 velocity model (Table 1), which is a modification of the surface-wave-derived MDJ model (B. Nguyen, written comm.). The theoretical NSSs for the earthquake and explosion are shown in Figures 3a and 4a, respectively, and the actual NSSs are shown in Figures 3b and 4b, respectively.

3. Discussion

The theoretical NSS can aid in the understanding of the potential of a given event scenario to constrain a particular type of source at a chosen level of fit. In the case of the Little Skull Mt. aftershock and the JUNCTION test, the best fit (VR = 100%) is as expected a double-couple and purely isotropic source, respectively (Figures S2a and 2a, respectively). But, the theoretical NSS can also show how well other sources fit the model event data. Figure 2a shows that a purely –CLVD (CLVD with a negative major axis) fits the model explosion data well, demonstrating that a shallow –CLVD at these low frequencies recorded at regional distances effectively mimics the radiation pattern of an explosion (Taylor et al., 1991). However, the region of high VR (>90%) in Figure 2a is well separated from a double-couple (DC) source. Another advantage to this type of error analysis is that one can define what ‘high VR’ means. In all theoretical cases we show VR regions that are 50, 75, 90, and 95% of the best-fit VR.

The actual NSS gives an idea of what sources can be resolved based on the true SNR. In the case of JUNCTION the high VR region encompasses a smaller area than the theoretical case, and an explosion source is even better constrained. To get an idea of why this difference may be, and what types of sources are contained in the high VR region, it is helpful to view the waveforms from the synthetic and actual sources. Figure 2c shows the data compared with three sources, the best-fit model (Best-fit model, VR = 74%), an example closest to a DC (Example, VR = 65%), and the best-fit DC (Best DC, VR = 56%). Unlike the pure explosion case, the data has signal on the tangential component. This energy cannot be fit well with –CLVD sources, so they are not represented in the VR>70% population (Figure 2b) as they are in the VR>95% population for the theoretical NSS (Figure 2a).

The Example model contains both DC and isotropic components and has a VR that is almost 10% less than the best-fit model, which is dominantly isotropic. The decrease in VR is in part due to the prediction of Love waves at stations LAC, BKS, and especially PFO, that are larger than observed. The Best DC model fits the observed waveforms very poorly. Not only does the Best DC model predict larger than observed Love waves, similar to the Example model, but the amplitudes of the Rayleigh waves are smaller than observed at stations LAC, ISA, and PFO. PAS provides an excellent constraint on this model, where amplitudes are far less than observed on all three components. This type of comparison is necessary in order to gain an understanding of how the VR relates to waveform misfit. Finally, it is important to note that an explosion (+V, Figure 2) has a VR that is very near the best-fit model and can fit the observed displacements to within a few percent of the best-fit VR.

Figure 3 gives the theoretical and actual NSSs for the earthquake in China, as well as the waveforms for the data, Best-fit, Example, and Explosion models for comparison. The actual NSS for the earthquake (Figure 3b) shows a well-constrained region similar to the theoretical NSS (Figure 3a). The waveforms of the best-fit model (VR = 67%), shown in Figure 3c, fit the data just as well as a pure DC. This result gives us confidence that the MDJ2 model is a good 1-D approximation of the velocity structure in this region, as the expectation is that the small earthquake should be well represented by a double-couple point-source.

The solution for the explosion in North Korea is much less constrained than the earthquake due to the simpler radiation pattern. Normally, we would run the inversion without GFs for station BJT because the epicentral distance is more than 1000 km and performance of the simpler 1-D velocity model employed here degrades at such great distances. However, preliminary inspection of the theoretical NSS without BJT showed that the solution could not satisfactorily exclude DC sources. Although this understanding could be gained from simple inspection of the station configuration shown in Figure 1b, where without BJT all stations fall along one azimuth with π periodicity (a condition that can always fit the two-lobed Rayleigh radiation pattern of a 45-degree dip-slip mechanism), the example is still instructive for cases that are not so easily visually inspected. With station BJT, the high VR region has the familiar shape from the JUNCTION test.

The addition of station BJT presents some additional problems for the actual NSS (Figure 4b). BJT is more than 1100 km away from the source, yet the displacement (2.24e-05 cm) is larger than that of station MDJ (2.04e-05 cm), which is only 371 km from the source. The usual method of weighting the data as a function of inverse distance caused the data from BJT to dominate the inversion, since there is only one station at this very great distance. As a corrective measure, we decreased the weight of data from BJT and produced the actual NSS in Figure 4b. As was stated in the discussion of the theoretical NSS, BJT is instrumental in constraining the source to be non-DC. Figure 4c shows that the Best DC model does not produce the observed Rayleigh amplitudes at BJT. Further, there is added confidence that the source is dominantly explosive because the Example mechanism, which fits the waveforms at a VR that is 3% less than the Best-fit model, produces a Love wave that is not observed at MDJ (Figure 4c).

The NSS can be used to investigate what stations would be most helpful in constraining the solution. Figure S3 shows the solution for the explosion in North Korea with the addition of data

recorded at a well-situated hypothetical station STAX (inverted triangle, Figure 1b). The highly explosive nature of the source is now better constrained. We also note that the best-fit explosion source (not shown) has an M_W of 3.6, which agrees with the results of Hong and Rhie (2008).

As is evident in the waveform plots of Figures 2-4, the surface wave energy is the dominant amplitude effect. However, the low-frequency body-wave train, Pnl, is very important in describing the source. In the future we will reweight the inversion so as to accentuate this part of the wavefield and thereby produce a better-constrained source.

5. Conclusion

Confidence in the best-fit solution for the regional full-waveform moment tensor inversion is dependent on station configuration, data bandwidth, and signal-to-noise ratio (SNR). The best way to characterize that dependence is on a case-by-case basis, where each individual event scenario is analyzed. The network sensitivity solution (NSS) attempts to do this characterization and is introduced and implemented for the NTS test, JUNCTION, as well as the Oct 06 North Korea test and a nearby earthquake in China. The theoretical network sensitivity solution provides solution confidence regions for ideal models (explosion or earthquake) with high SNR data. With this type of network sensitivity solution, one can learn if the station configuration and bandwidth is sufficient to resolve a given model. The actual network sensitivity solution assesses confidence using the actual data from the event. Goodness-of-fit for each model is parameterized with a percent variance reduction (VR), where the complete VR space can be mapped out on a source-type plot and the well-fit region of solutions is defined by a chosen threshold VR.

The theoretical network sensitivity solutions for JUNCTION and the North Korea test show a trade-off between –CLVD and explosion, but the well-fit solution space is separated from a double-couple, indicating that an anomalous event can be resolved. In the case of the North Korea test, a specific configuration using the very distant station BJT is required to rule out a DC solution. The actual network sensitivity solution of JUNCTION provides good confidence in the large isotropic component obtained from the inversion. With some additional data weighting, the actual network sensitivity solution of the North Korea test also shows a tight region of well-fit solutions clustered between an opening crack and an explosion, though with the addition of just one more imaginary station, this region is made much smaller. The network sensitivity solutions for the earthquake in China provide high confidence in the best-fit solution, which is indistinguishable for a double-couple. This analysis gives us confidence in the velocity model used to create GFs for the inversion.

In the future, we can assess variance in the solution caused by a poorly constrained velocity model by incorporating many hundreds of velocity models for the region obtained from a prior probabilistic study of the source area (e.g., Pasyanos et al., 2006). A best-fit solution can be obtained using each velocity model. This population of best-fit solutions based on variance in the velocity model can then be combined with spatial and temporal event uncertainty to produce network sensitivity solutions and more completely characterize confidence in a given solution.

Acknowledgements

This is LLNL contribution LLNL-JRNL-XXXX and BSL contribution 09-XX. Portions of this work were prepared by UCB under DOE Contract DE-FC52-06NA27324, and by LLNL under Contract DE-AC52-07NA27344.

References

Bonner, J., R. B. Herrmann, D. Harkrider, and M. Pasyanos (2008), The Surface Wave Magnitude for the 9 October 2006 North Korean Nuclear Explosion, Bull. Seis. Soc. Amer., 98 (5), 2498-2506, doi:10.1785/0120080929.

Dufumier, H. and L. Rivera (1997), On the resolution of the isotropic component in moment tensor inversion, Geophysical Journal International, 131, 595-606.

Ford, S. R., D.S. Dreger, and W. R. Walter, (2009). Identifying isotropic events using a regional moment tensor inversion, J. Geophys. Res., 114 B01306, doi:10.1029/2008JB005743.

Hong, T.-K. and J. Rhie (2008), Investigation of regional source properties of the underground nuclear explosion in North Korea, 30th Monitoring Research Review, Portsmouth, USA.

Hudson, J. A., R. G. Pearce, R. G., and R. M. Rogers (1989). Source type plot for inversion of the moment tensor, J. Geophys. Res., 9(B1), 765-774.

Jechumtalova, Z. and J. Sileny (2001), Point-source parameters from noisy waveforms: Error estimate by Monte-Carlo simulation, Pure Appl. Geophys., 158, 1639-1654.

Jechumtalova, Z. and J. Sileny (2005), Amplitude ratios for complete moment tensor retrieval, Geophys. Res. Lett., 32, L22303, doi:10.1029/2005GL023967.

Minson, S. and D. Dreger (2009), Stable Inversions for Complete Moment Tensors, In press Geophys. Journ. Int.

Pasyanos, M.E., G.A. Franz, and A.L. Smith (2006), Reconciling a geophysical model to data using a Markov chain Monte Carlo algorithm: An application to the Yellow Sea - Korean Peninsula region, J. Geophs. Res., 111 (B03313), doi:10.1029/2005JB003851

Riedesel, M. and T. H. Jordan (1989), Display and assessment of seismic moment tensors, Bulletin of the Seismological Society of America, 79, 85-100.

Roessler, D., F. Krueger, and G. Ruempker (2007), Retrieval of moment tensors due to dislocation point sources in anisotropic media using standard techniques, Geophysical Journal International, 169, 136-148.

Sileny, J. (1998), Earthquake source parameters and their confidence regions by a genetic algorithm with a 'memory', Geophysical Journal International, 134, 228-242.

Sileny, J. (2004), Regional moment tensor uncertainty due to mismodeling of the crust, Tectonophysics, 383, 133-147.

Sileny, J., P. Campus, and G. F. Panza (1996), Seismic moment tensor resolution by waveform inversion of a few local noisy records; I, Synthetic tests, Geophysical Journal International, 126, 605-619.

Sileny, J., G. F. Panza, and P. Campus (1992), Waveform inversion for point source moment tensor retrieval with variable hypocentral depth and structural model, Geophysical Journal International, 109, 259-274.

Song, X. J., D. V. Helmberger and L. Zhao (1996). Broad-band modelling of regional seismograms; the basin and range crustal structure, Geophys. J. Int., 125(1), 15-29.

Taylor, S. R., J. T. Rambo, and R. P. Swift (1991), Near-source effects on regional seismograms: An analysis of the NTS explosions PERA and QUESO, Bull. Seis. Soc. Amer. 81 (6), 2371-2394.

Walter, W. R., K. D. Smith, J. L. O'Boyle, T. F. Hauk, F. Ryall, S. D. Ruppert, S. C. Myers, R. Abbot, D. A. Dodge, (2006). An assembled western United States dataset for regional seismic analysis, Lawrence Livermore National Laboratory, UCRL-MI-222502. CR-ROM available upon request.

Weber, Z. (2006), Probabilistic local waveform inversion for moment tensor and hypocentral location, Geophysical Journal International, 165, 607-621.

Figures

Figure 1. a) Map of the Western US with the Nevada Test Site (NTS) outlined and the location of the Little Skull Mt. aftershock (diamond) and NTS test, JUNCTION (star). Stations used in the Little Skull Mt. and JUNCTION analysis are also shown with inverted and normal triangles, respectively, along with their names. b) Map of the Yellow Sea / Korean Peninsula with the North Korea test (5-point star) and nearby earthquake (diamond) as well as the stations used in their analysis (triangles). A synthetic station (STAX) used in the sensitivity analysis is also shown with an inverted triangle.

Figure 2. Network sensitivity solution (NSS) for the NTS nuclear test, JUNCTION (26 Mar 92). a) Theoretical NSS for an explosion where the Green's functions are derived from the actual JUNCTION network setup and there is no noise in the data. The best-fit model is an explosion (+V) with a Variance Reduction (VR) of 100%. Empirical distributions of other models and the corresponding VR are also given via contours on the source-type plot. b) Actual NSS using data from JUNCTION test. The best-fit model with a VR of 74% along with other models and the corresponding VR distributions are shown. For comparison, an Example model (VR = 65%) and a Best DC model (VR = 56%) are also plotted and correspond with the models and waveforms given in c). c) Models corresponding to those plotted in b) and their respective forward-predicted waveforms as a function of color compared with the actual waveforms (black line). The left, middle, and right columns are the tangential (T), radial (R), and vertical (V) displacement waveforms, respectively. The text block to the left of the waveforms gives the station name, passband period (s), azimuth, epicentral distance (km), and maximum displacement (cm). The moment magnitudes of the models are also given below the mechanism.

Figure 3. Network sensitivity solution (NSS) for an earthquake (16 Dec 04) in near the North Korea test location. a) Theoretical NSS using one hundred earthquakes with a uniform distribution of fault parameters where the Green's function are derived from the actual network setup and the data is noiseless. The best-fit model is a pure double-couple (DC) with a VR of 100%. Empirical distributions of other models and the corresponding VR are also given via contours on the source-type plot. b) Actual NSS using data from the China earthquake. The best-fit model with a VR of 67% along with other models and the corresponding VR distributions are shown. For comparison, an Example model (VR = 50%) and a pure Explosion model (VR = 13%) are also plotted and correspond with the models and waveforms given in c). c) Models corresponding to those plotted in b) and their respective forward-predicted waveforms as a function of color compared with the actual waveforms (black line). The left, middle, and right columns are the tangential (T), radial (R), and vertical (V) displacement waveforms, respectively. The text block to the left of the waveforms gives the station name, passband period (s), azimuth, epicentral distance (km), and maximum displacement (cm). The moment magnitudes of the models are also given below the mechanism.

Figure 4. Network sensitivity solution (NSS) for the North Korea test (9 Oct 06, m_b4.2). a) Theoretical NSS for an explosion where the Green's functions are derived from the actual network setup and the data is noiseless. The best-fit model is an explosion with a VR of 100%. Empirical distributions of models and their corresponding VR are also given via contours on the source-type plot. b) Actual NSS using data from the North Korea test. The best-fit model with a

VR of 55% along with other models and the corresponding VR distributions is shown similar to a). For comparison, an Example (VR = 52%) and a Best DC model (VR = 44%) are also plotted and correspond with the models and waveforms in c). c) Models corresponding to those plotted in b) and their respective forward-predicted waveforms as a function of color compared with the actual waveforms (black line). The left, middle, and right columns are the tangential (T), radial (R), and vertical (V) displacement waveforms, respectively. The text block to the left of the waveforms gives the station name, passband period (s), azimuth, epicentral distance (km), and maximum displacement (cm). The moment magnitudes of the models are also given below the mechanism.

Figure S1. Synthetic sources. a) Distribution of earthquake model event parameters. b) Source-type plot of synthetic source distribution. Gray scale gives the 0.1-unit smoothed number of events, and the white box outlines the sources described in c). c) Parameters of the synthetic sources contained in the white box in b).

Figure S2. Network sensitivity solution (NSS) for an aftershock of the Little Skull Mt. a) Theoretical NSS using one hundred earthquakes with a uniform distribution of fault parameters where the Green's function are derived from the actual network setup and the data is noiseless. The best-fit model is a pure double-couple (DC) with a VR of 100%. Empirical distributions of other models and the corresponding VR are also given via contours on the source-type plot. b) Actual NSS using data from the event. The best-fit model with a VR of 89% along with other models and the corresponding VR distributions are shown. For comparison, an Example model (VR = 66%) and a pure Explosion model (VR = 1%) are also plotted and correspond with the models and waveforms given in c). c) Models corresponding to those plotted in b) and their respective forward-predicted waveforms as a function of color compared with the actual waveforms (black line). The left, middle, and right columns are the tangential (T), radial (R), and vertical (V) displacement waveforms, respectively. The text block to the left of the waveforms gives the station name, passband period (s), azimuth, epicentral distance (km), and maximum displacement (cm). The moment magnitudes of the models are also given below the mechanism.

Figure S3. Network sensitivity solution (NSS) using actual data for the North Korea test with the addition of a synthetic station, STAX (see Figure 1b). As compared to Figure 4, the high VR region is now more constrained.

Tables

Table 1. MDJ2 velocity model

Thick (km)	V_α (km/s)	V_β (km/s)	ρ (g/cc)	Q_α	Q_β
1	5.35	3.09	2.57	600	300
8	5.81	3.35	2.66	600	300
20	6.27	3.62	2.78	600	300
∞	7.91	4.37	3.17	600	300

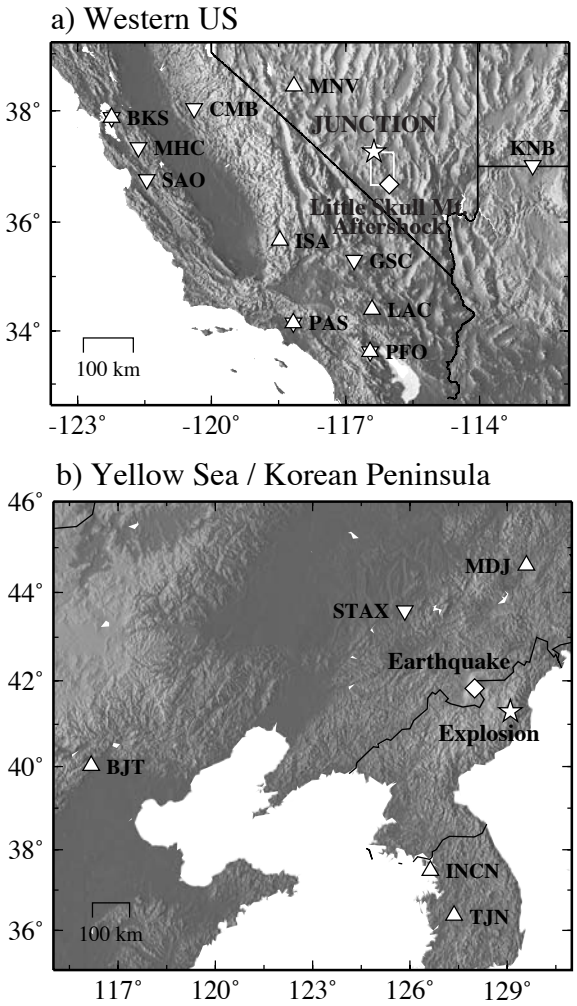

Figure 1
1 column, b/w
Ford et al., 2009
Version 4

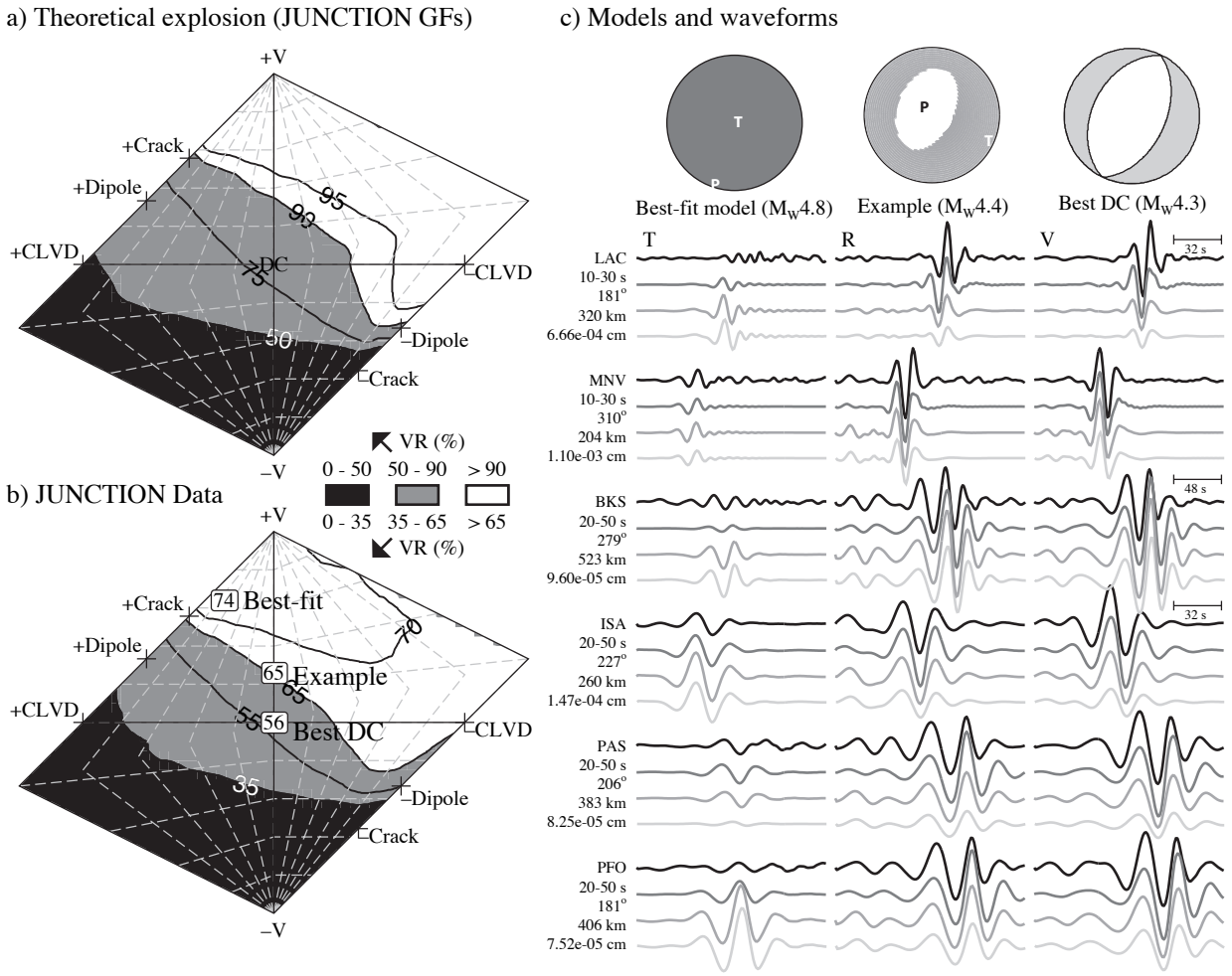

Figure 2
2 column, b/w
Ford et al., 2009
Version 3

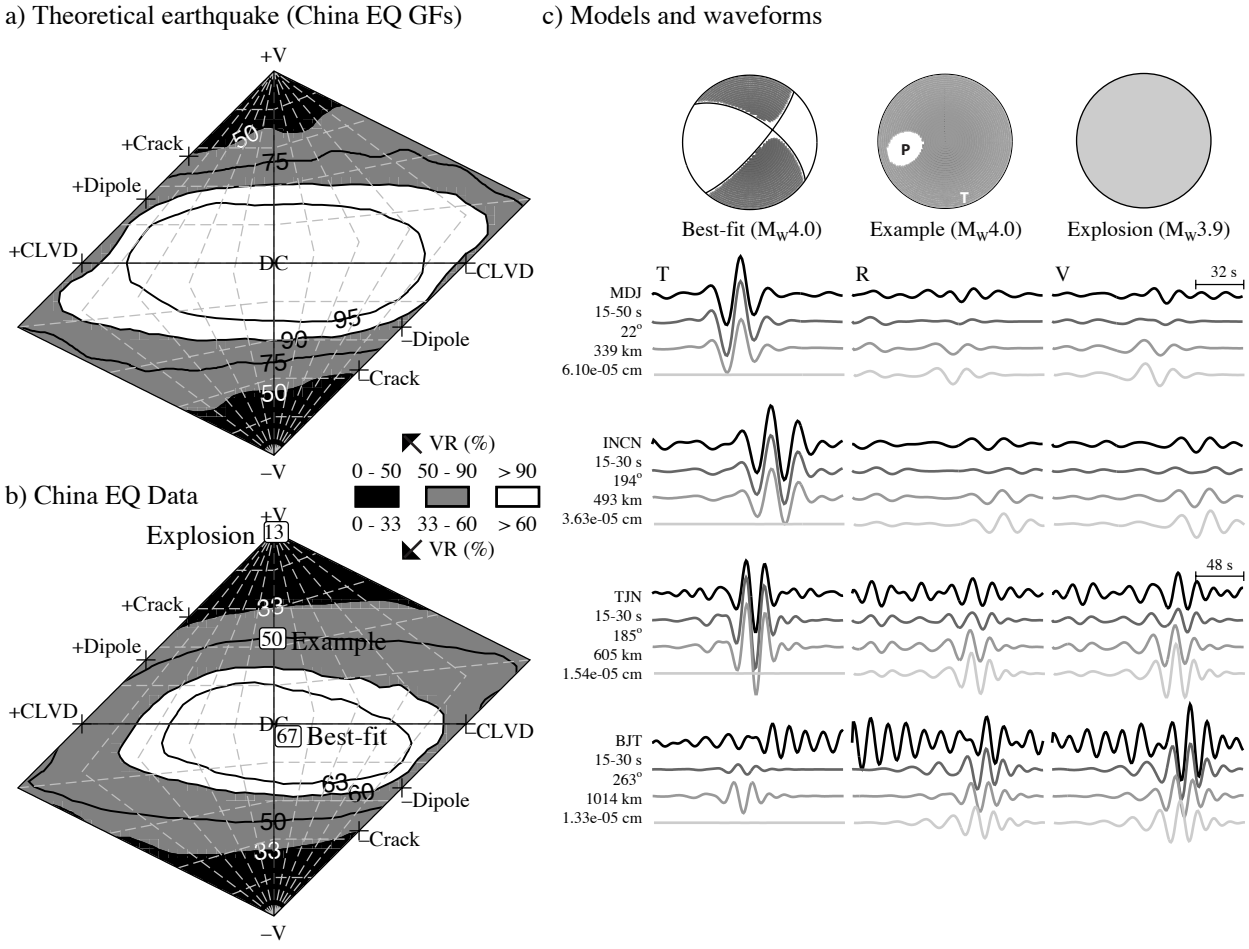

Figure 3
2 column, b/w
Ford et al., 2009
Version 4

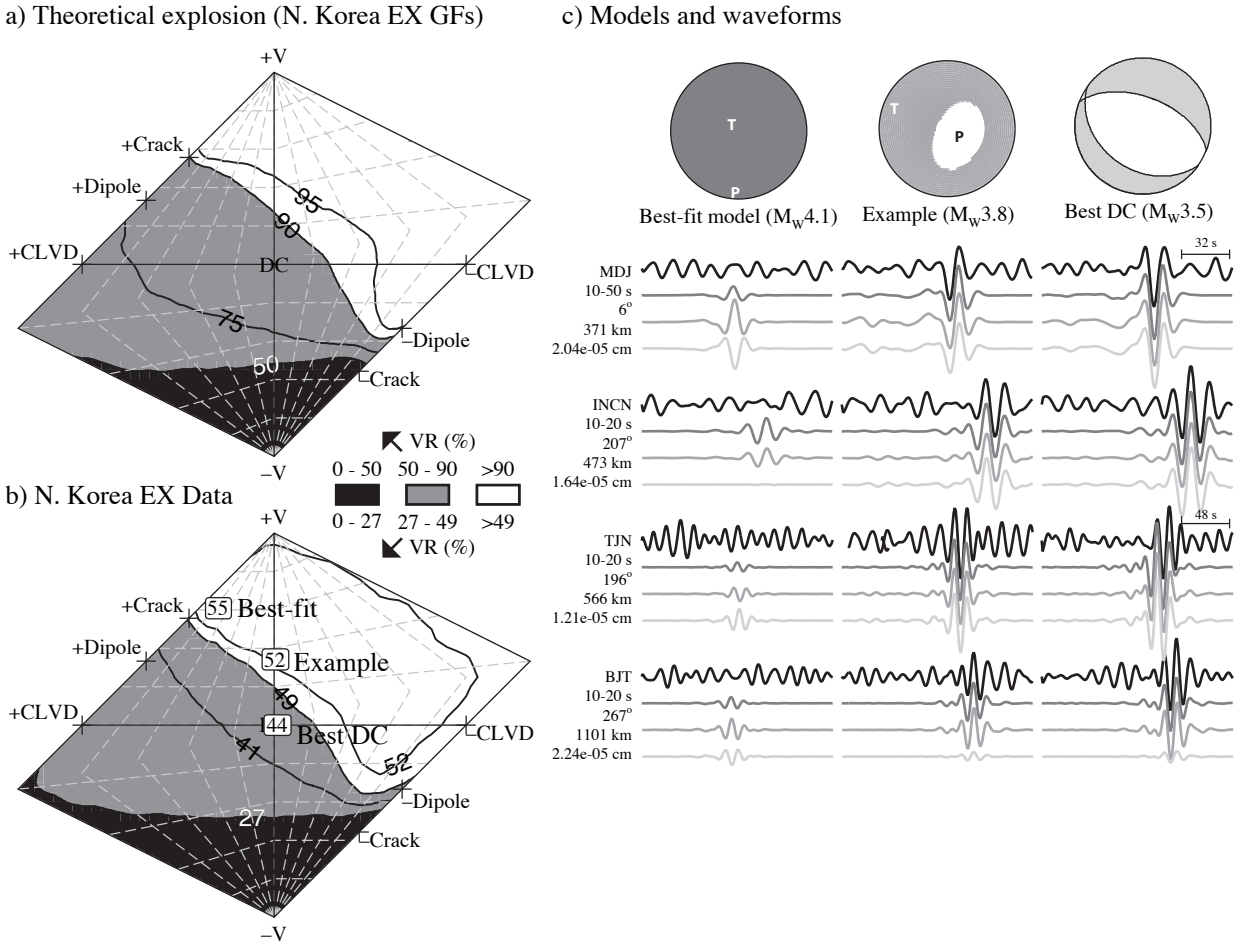

Figure 4
2 column, b/w
Ford et al., 2009
Version 3

a) DC model events (Mw5)

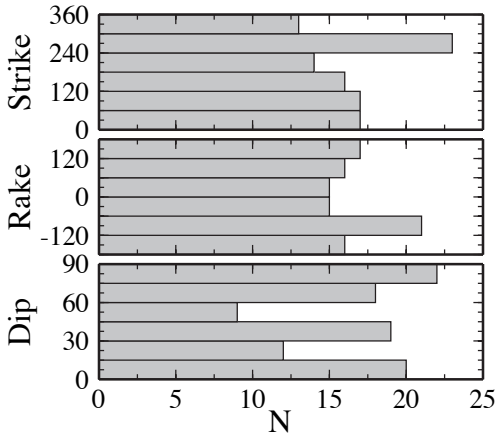

b) Synthetic sources distribution (Explosion)

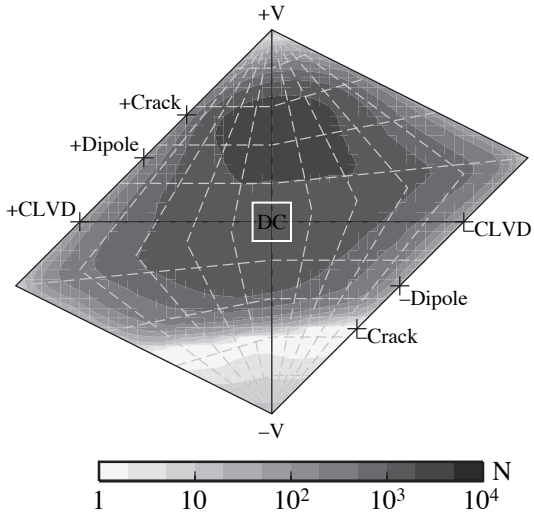

c) Synthetic source parameters

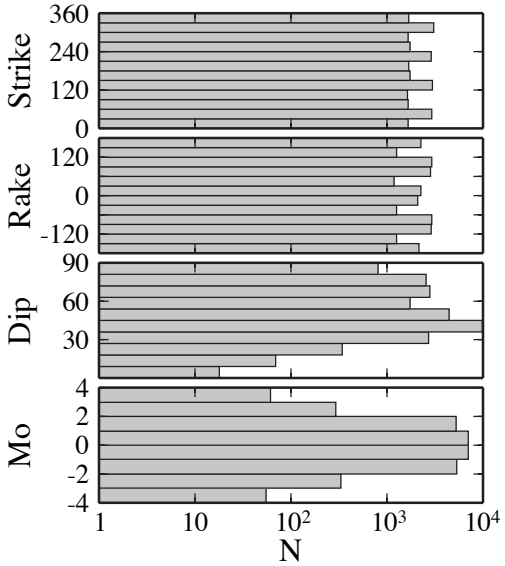

Figure 1 Supp
1 column, b/w
Ford et al., 2009
Version 1

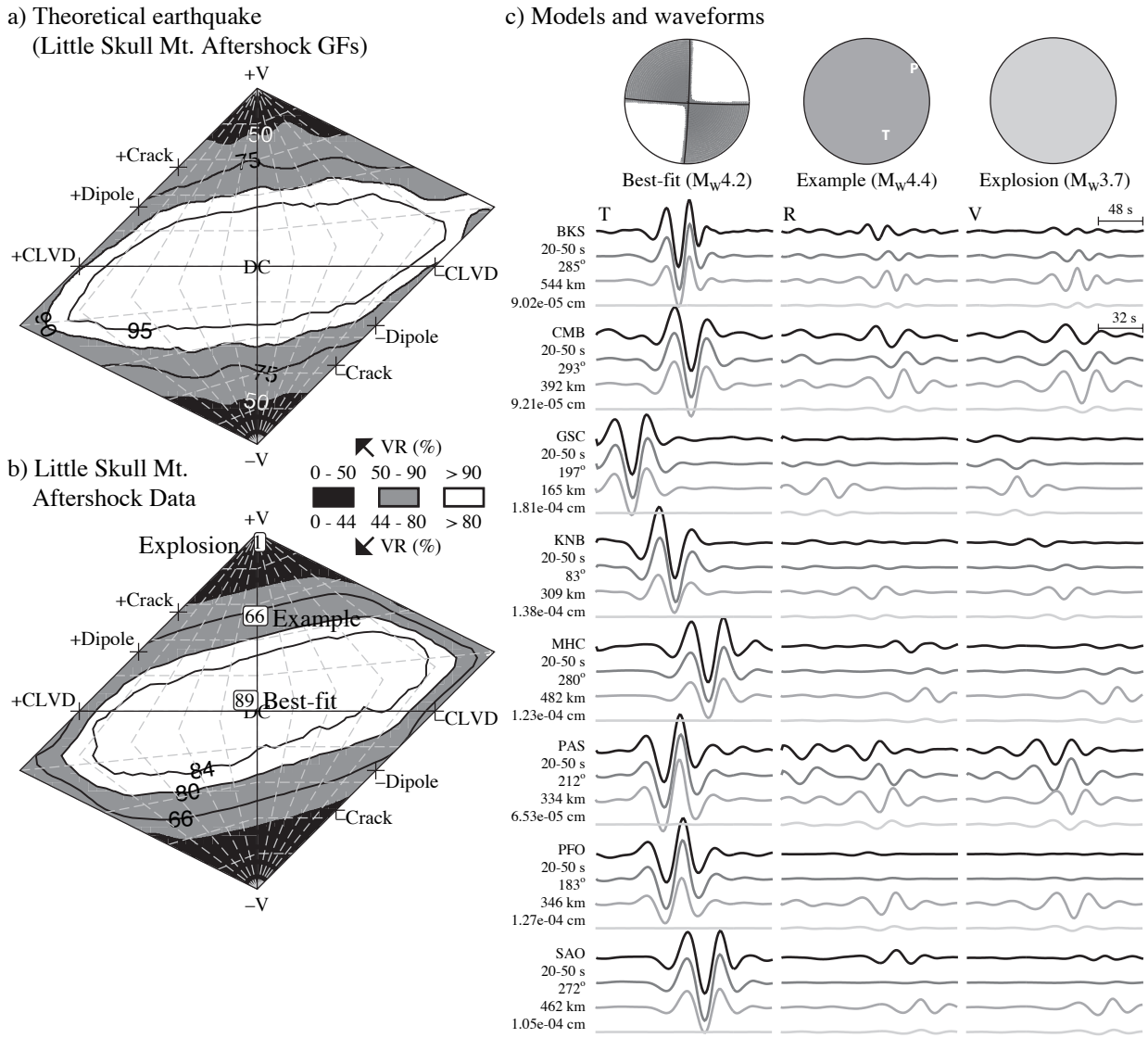

Figure 2 Supp
2 column, b/w
Ford et al., 2009
Version 2

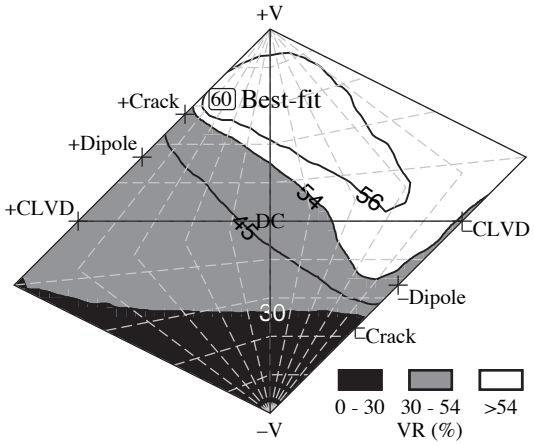

Figure 3 Supp
1 column, b/w
Ford et al., 2009
Version 1